Evolving Morphologies for Locomoting Micro-scale Robotic Agents

Matthew Uppington[1], Pierangelo Gobbo[2], Sabine Hauert[3], Helmut Hauser[4]

***Abstract*— Designing new locomotive mechanisms for micro-scale robotic systems could enable new approaches to tackling problems such as transporting cargos, or self-assembling in to pre-programmed architectures. Morphological factors often play a crucial role in determining the behaviour of micro-systems, yet understanding how to design these aspects optimally is a challenge. This paper explores how the morphology of a multi-cellular micro-robotic agent can be optimised for reliable locomotion using artificial evolution in a stochastic simulator. Evolved morphologies are found to yield significantly better performance in terms of the reliability of the travel direction and the distance covered, compared to random morphologies.**

I. INTRODUCTION

Locomotion is a crucial ability for micro-scale systems, particularly in applications that involve the transportation of cargos, like medicines, and self-assembling in pre-programmed architectures. Our ability to produce micro-scale systems composed of multi-cellular units ([1], [2]) and functionalise them ([3], [4]) have seen several advancements in recent years. Other breakthroughs with developing and understanding contractile protocells and light-based testing environments bring the promise of light-controllable, mobile micro-robots closer to reality ([5], [6]).

Yet, understanding how to design optimal morphologies for micro-scale robots that produce behaviours such as locomotion is still an open question. Morphology in this context refers to the specific form or structure of a robot or group of robots ([7], [8]). Artificial evolution has been used to search for optimal robot morphologies in many studies ([9], [10]).

Exploring the potential abilities of such systems in simulation is a vital first step towards eventually deploying new micro-robots in real-world applications. In this paper, we propose a system of micro-scale cellular units that can expand and contract in response to a light-based stimulus, as shown in Figure 1. This is inspired primarily by the works of Gobbo et al. and Downs et al., where they present similar forms of actuation with protocells and hydrogel structures respectively ([5], [4]). Using light as a control medium is advantageous for independently and precisely targeting micro-scale agents ([11]). This can be achieved with technology such as the Dynamic Optical Micro Environment (DOME, [6]), which provides an affordable, open source platform for testing light reactive agents with closed loop control of light patterns. As a first step, we optimise the morphology of a collection of contractile cells in simulation.

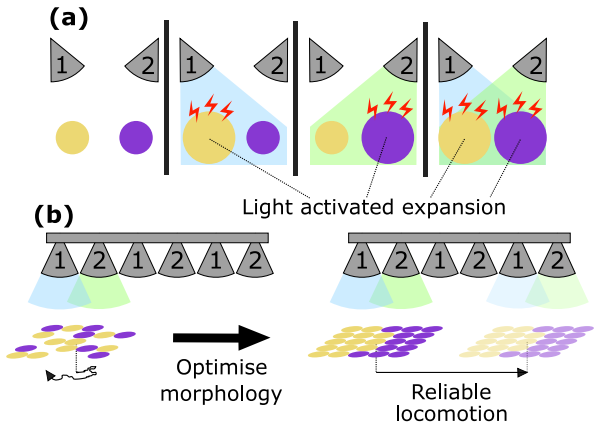

Fig. 1. **(a)** Conceptual illustration of micro-scale, light-reactive, contractile cellular units – different cells expand when exposed to specific wavelengths of light. **(b)** By using artificial evolution in a stochastic simulator, we seek to optimise the morphology of a connected group of cells to allow locomotion in a reliable direction.

In the next section we summarise some previous works related to how locomotion has been achieved with micro-robots, how their morphologies can be optimised and the available methods for simulating them.

II. RELATED WORK

A. Micro-robot Locomotion

Locomotion has been achieved in micro-robots through a variety of different methods. Downs et al. presented a multi-responsive hydrogel structure that exemplifies several techniques being used together, including light, temperature and magnetism ([4]). Miskin et al. demonstrated light-based control with micro-swarming robots that locomote when top-mounted photo-voltaic receptors are targeted with light lasers ([11]). Due to the high resolution that is achievable with laser targeting, each individual micro-robot in the swarm can be controlled independently. Lv et al. also use light to manipulate individual micro-particles, or aggregate large groups of micro-particles into a local area with Light Activated Marangoni Tweezers (LAMT), though only in the presence of a photosurfactant solution ([12]).

This work is supported by the EPSRC Robotics and Autonomous Systems Centre for Doctoral Training (FARSCOPE) (UKRI Grant No. EP/S021795/1) (M.U).

[1]Matthew Uppington is with the FARSCOPE CDT, Bristol Robotics Laboratory, University of Bristol, University of West England, UK. mu15531@bristol.ac.uk

[2]Pierangelo Gobbo is with the Department of Chemical and Pharmaceutical Sciences, University of Trieste, Italy.

[3]Sabine Hauert is with the Department of Engineering Mathematics, Bristol Robotics Laboratory, University of Bristol, UK. sabine.hauert@bristol.ac.uk

[4]Helmut Hauser is with the Department of Engineering Mathematics, Bristol Robotics Laboratory, University of Bristol, UK.

B. Optimisation of Morphologies

With an ever increasing arsenal of materials to functionalise micro-scale systems, the task of optimising their design for a particular function, such as locomotion, is challenging. Even with just a small set of building blocks, the range of possible combinations to construct morphologies makes it difficult to search efficiently for optimal solutions. One solution is artificial evolution, which is a machine learning technique that has a long history of being applied to optimising the design and behaviour of robots ([13]). Mautner and Belew showed how robot morphology could be evolved in parallel with a controller in simulation ([9]). Since then, a similar concept of simultaneously evolving morphology and controller has been applied to physical robots ([10]).

One challenge is being able to bridge the reality gap between morphologies evolved in simulation and morphologies produced in the real world. In the microscopic domain, Kriegman et al. presented a solution for a scalable process for designing and producing mobile morphologies using artificial evolution ([2]). Morphologies were optimised for locomotion by measuring performance in terms of total displacement achieved in simulation during a given time. Whilst this does produce mobile micro-robots, called Xenobots, their trajectories cannot be controlled by external factors (such as light). Kriegman et al. also note the importance of testing high performing (simulation) morphologies in the presence of noise, in order to filter out which simulated morphologies are likely to perform well in the real world ([2]).

C. Cellular Simulators

The choice of simulation environment has a significant impact on how systems can be represented and, therefore, how they can be optimised with artificial evolution. The *BSim* simulator, described by Gorochowski et al., allows collective behaviours of agent-based, micro-scale systems to be modelled in complex environments, though it is specifically designed to model bacterial cells ([14]). Kriegman et al. defined morphologies for Xenobots in simulation using a voxel grid ([2]). Voxel grids allow virtual organisms to be constructed out of 3-dimensional arrays of customisable, cubic building blocks ([15]). While voxel grids are an intuitive and effective strategy, other simulation environments are better tailored to modelling micro-scale systems.

Cickovski et al. introduced *CompuCell3D* as a flexible simulation environment for micro-scale, cellular systems ([16]). The underlying model is Cellular Potts; a powerful, generalised framework for simulating micro-scale systems using a pixel grid ([17]). Cellular Potts models are intrinsically stochastic meaning that the need to introduce noise, as highlighted by Kriegman et al., is satisfied naturally. In addition, CompuCell3D provides a powerful Python based interface, with built-in optimisation tools to manage CPU usage and modular run-time functionalities. These are desirable features for balancing computational speed versus complexity when running demanding artificial evolution algorithms and, therefore, was chosen as our simulation environment. The next section describes how our protocell-like contractile cells were simulated using CompuCell3D.

III. METHOD

A. Contractile Cell Model

We use CompuCell3D to define a Cellular Potts model of a connected group of cells. In Cellular Potts models, cells are represented by a region of pixels within a grid and the simulation is progressed incrementally in Monte Carlo Steps (MCS), which are stochastic; in each MCS, each pixel in the grid attempts to copy their value to a nearby pixel with some probability of success. The core principle behind Cellular Potts models is that interactions between entities can be defined in terms of energy equations that determine the probability of successful pixel copies ([17]).

We assume that each cell is able to increase its radius up to a user defined maximum when exposed to a stimulating control signal. So, we introduce an energy equation to control the length of a cell in its primary (longest) axis and secondary (orthogonal to primary) axis. We take a hypothetical $10\mu m$ wide protocell at room temperature as inspiration for the width of a cell when unstimulated, as introduced by Gobbo et al. ([5]). The stochasticity in Cellular Potts models will mean that the exact shape of a given cell will change slightly with each simulation step. To ensure a cell does not deviate unrealistically from roughly uniform shapes (circular in 2D), additional energy equations are included to govern the perimeter and surface area of the cell as a function of its radius. To ensure neighbouring cells remain connected, the ideal distance between their centres of mass is defined as the sum of their radii. Note that these connections, referred to as focal point plasticity links, are loose, meaning that cells can freely rotate about other cells, unless otherwise constrained. In addition, to prevent cells from being absorbed in to each other, energy equations are introduced to apply a small repulsive force between pixels belonging to different cells. The balance of these interactions allows cells to stay physically connected at their surface, whilst each maintaining integrity and roughly uniform shapes.

B. Evolutionary Setup

To explore a large space of possible morphologies, analytical methods quickly become infeasible. Artificial evolution provides a solution, by starting with a batch of random morphologies, called the initial population or first generation. These morphologies are compared and ranked using a performance metric called a fitness score - a numerical value indicating how well they locomote (see Equation 1). A new generation can then be created by replacing poorly performing morphologies with random combinations of the better performing morphologies (crossover), sometimes with random changes (mutations). The best morphologies from one generation are often carried over to the next generation unaltered. By iteratively repeating this process for subsequent generations the average performance of morphologies can be gradually increased over multiple generations.

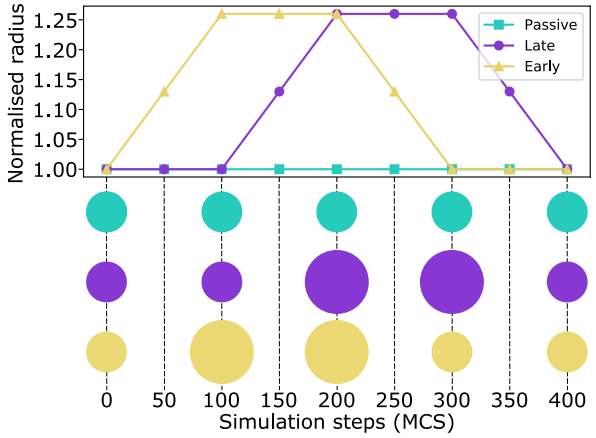

Fig. 2. Graph showing asynchronous control signals with a period of 400 simulation steps (MCS). The early (yellow) and late (purple) signals cause cells radii to oscillate between a normalised minimum value, and a maximum value (≈ 1.26, inspired by protocell transition between contracted and expanded states [5]). Passive cells (turquoise) are not stimulated.

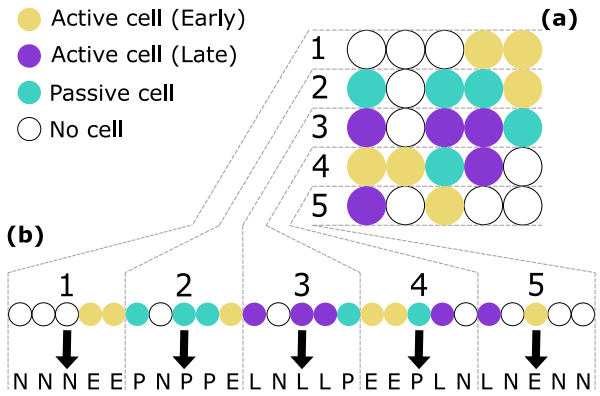

Fig. 3. Diagram showing how a random morphology with a 5×5 Cartesian grid structure can be represented as a genome of length $G = 25$. First, each row of cells is listed in order, starting from the top, moving down the grid **(a)**. Each cell state in the ordered list is then represented with an index **(b)**: 'E' = early actuating cell (yellow), 'L' = late actuating cell (purple), 'P' = passive cell (turquoise), and 'N' = no cell (white). Any compatible morphology can be uniquely re-constructed from such a genome by reversing the process outlined above.

To establish the search space of morphologies, we arrange the initial positions of cells into a 5×5 Cartesian formation, as shown in Figure 3. Each position can either be occupied by one of four cell types that we define as follows: a passive cell that always stays at its minimum radius and does not change size; an early actuating cell that oscillates between its minimum and maximum radius over time; a late actuating cell that is functionally identical to an early actuating cell except for a phase difference in the oscillations; and finally a 'no cell' type that denotes an empty gap in the morphology. Two distinct active cell types are defined in order to allow cells to be actuated at different times. Figure 2 shows the models used for each active cell type over the course of an actuation cycle. Figure 3 illustrates how morphologies are encoded by listing rows of cell states, represented by letters, from top to bottom. This allows the morphologies in the 5×5 Cartesian format to be uniquely expressed as 'genomes' consisting of 25 characters ('genes').

C. Performance Metric

The goal of optimisation is to find the morphologies that display the furthest and most reliable locomotion. The locomotive performance of a morphology can be quantified using the displacement of the morphology's centre of mass after a given number of simulation steps. To drive locomotion, the radii of each cell in a given morphology is varied according to their type, as shown in Figure 2, over one actuation cycle, which corresponds to 400 MCS. Given the stochastic nature of Cellular Potts models, tracking the average performance not just over multiple actuation cycles, but also over multiple independent simulations provides a more valuable description of the morphology's expected behaviour. So, running K simulations of a given morphology over T actuation cycles provides us with a set of independently sampled vectors, $\mathbf{v}_1, ..., \mathbf{v}_K$. These vectors describe the displacement between the morphology's starting position and it's final position at the end of the simulation. To optimise only over the total distance covered we could simply take the average magnitude of these vectors, i.e., $D = \frac{1}{K}\sum_{j=1}^{K} |\mathbf{v}_j|$. However here, in order to also encourage morphologies to travel in a reliable direction, we want to minimise the variation over the direction. To optimise over both of these criteria simultaneously during artificial evolution, we define the following fitness function,

$$F = \frac{1}{T}\left|\sum_{j=1}^{K} \frac{\mathbf{v}_j}{K}\right| . \tag{1}$$

We divide by T to average over the number of actuation cycles that morphologies are simulated for. By taking the magnitude of the averaged vector, morphologies are penalised for travelling in random directions, but rewarded for travelling further in similar directions in each run. Note that this fitness function is bounded by the average distance covered, $F \leq \frac{D}{T}$, since $\left|\sum_{j=1}^{K} \mathbf{v}_j\right| \leq \sum_{j=1}^{K} |\mathbf{v}_j|$. This maximum limit is approached as the standard deviation in travel directions $\sigma = \sqrt{\frac{1}{K}\sum_{j=1}^{K} \left(\theta_j - \bar{\theta}\right)^2}$ approaches zero, where $\bar{\theta} = \frac{1}{K}\sum_{j=1}^{K} \theta_j$ is the average of the recorded travel directions, θ_j. With a fitness function and evolutionary setup defined, we explore the results of artificial evolution trials in the next section.

IV. RESULTS

To generate an initial population of morphologies for the artificial evolution algorithm, 32 randomly generated genomes were created. During evolution, each genome was tested by simulating its morphology for $T = 10$ actuation cycles. This was repeated $K = 4$ times, to generate a sample of displacement vectors. When analysing the performance of specific morphologies in more detail after evolution, we simulate morphologies for $T = 50$ actuation cycles, over $K = 10$ independent runs. When progressing from one generation to the next, we selected the top 6 best performing

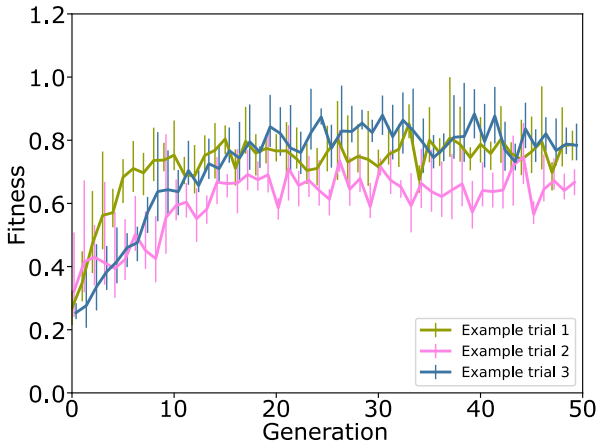

Fig. 4. Graph showing the range (vertical bars) and average of the top 20% of recorded fitness values per generation for 3 artificial evolution trials. In each generation, each genome is simulated for $T = 10$ actuation cycles, over $K = 4$ independent runs. Fitness is calculated according to Equation 1.

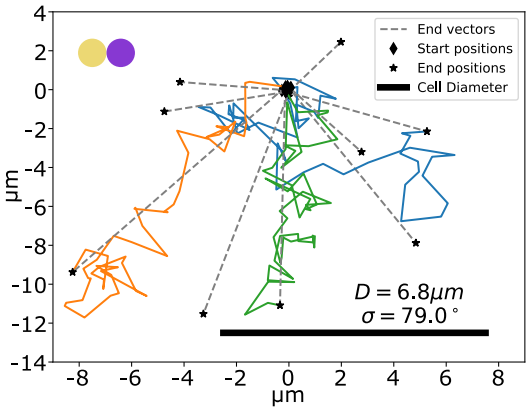

Fig. 5. Sampled displacement vectors of the centre of mass of a two-cell morphology (see top left). Vectors are measured after $T = 50$ actuation cycles, in $K = 10$ independent runs for each morphology. Some typical trajectories of each morphology's centre of mass are also shown (orange, green and blue). The black scale bars show the diameter of one unstimulated cell. D is the average distance covered, σ is the standard deviation in travel direction.

genomes to be retained and the worst 13 genomes were overwritten with random sequences of cell states. The remaining 13 genomes were each replaced by randomly selecting a pair of retained, high performing genomes (selected from the best 6) and creating a new genome in which each cell state is copied from one of the two 'parent' genomes uniformly at random.

It was found that 50 generations was sufficient to allow fitness values to increase significantly and morphologies to converge. The top 20% of recorded fitness values in a sample of three typical runs of artificial evolution is shown in Figure 4. The best performing genomes show rapid increase in fitness values for early generations with a plateau being reached by around 30 generations. At this point, evolved morphologies seem to have achieved roughly a 3 to 4 fold increase in fitness score, compared to the initial population of random morphologies.

Figure 5 shows a sample of displacement vectors and recorded trajectories for a minimal, baseline morphology consisting of just two cells - one of each active type. Figures 6, 7 and 8 show examples of high performing evolved morphologies from independent evolution trials. In general, the trajectories of the evolved morphologies are able to travel farther than the two-cell morphology. The average distances covered by the evolved morphologies shown range between $21.7\mu m - 36.1\mu m$, compared to the average distance recorded for the two-cell morphology, $6.8\mu m$. Moreover, the measured standard deviation in travel direction is significantly lower for the evolved morphologies, ranging between $24.2° - 30.1°$, than for the two-cell morphology, $79.0°$. This demonstrates that the evolved morphologies are able to more consistently travel in a predictable direction.

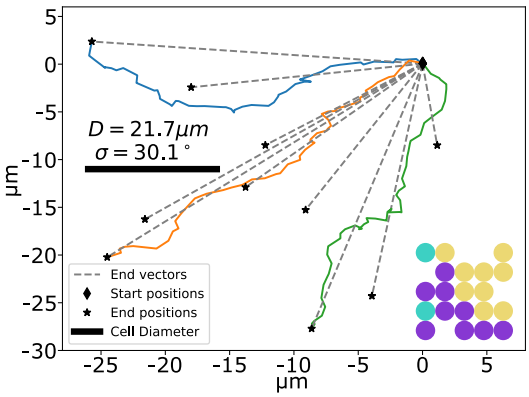

Fig. 6. Sampled displacement vectors of the centre of mass of an evolved morphology (see bottom right) from independent trial 1. Notation and simulation parameters are as described in Figure 5.

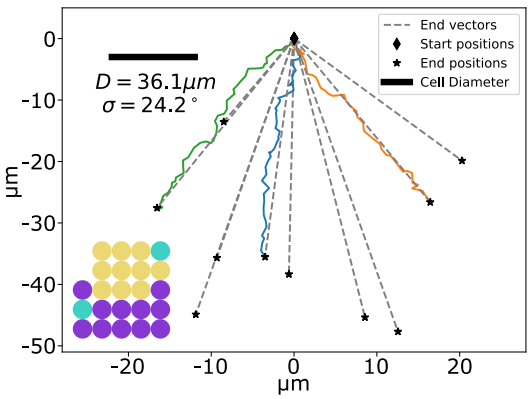

Fig. 7. Sampled displacement vectors of the centre of mass of an evolved morphology (see bottom left) from independent trial 2. Notation and simulation parameters are as described in Figure 5.

V. DISCUSSION

There are several observations that can be made about the evolved morphologies shown that could potentially inspire future designs for micro-scale robots. Firstly, the found morphologies mainly consist of active cell types, with the passive

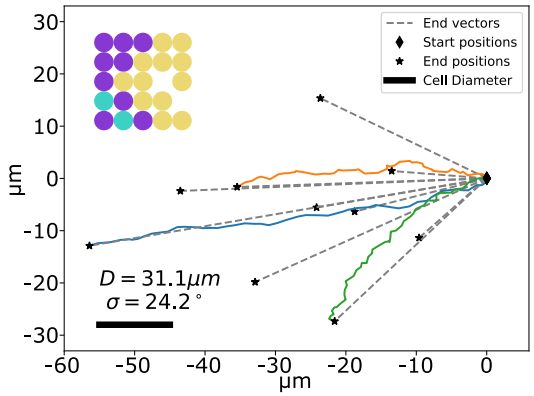

Fig. 8. Sampled displacement vectors of the centre of mass of an evolved morphology (see top left) from independent trial 3. Notation and simulation parameters are as described in Figure 5.

and 'no cell' states being far less common. This suggests that the purely structural contribution of passive or absent cells to a morphology is generally outweighed by the increased locomotive potential offered from active cell types, when it comes to generating larger and more reliable displacements. However, the existing passive or 'no cell' states could also be interpreted as a sign of robustness to defects. For example, an active cell that loses its sensitivity to light would effectively become a passive cell, or a morphology that suffers physical damage may lose some cells by becoming detached. Future studies could look to investigate this further to examine the robustness of morphologies to different modes of failure.

Secondly, we see that 'late' (purple) and 'early' (yellow) active cell types seem to define front and back sections of evolved morphologies, with respect to the direction of motion. However, this does not seem to generalise well to the two-cell morphology. This suggests that the interactions of just two active cells are dominated instead by the inherent noise in the stochastic simulator, unlike the larger evolved morphologies. Continuations of this work could experiment with different fitness scores that penalise greater numbers of cells, or experiment with generalising to larger scale morphologies in order to explore the relationship between relative size and reliability in travel direction. Future research could also investigate more general actuation schemes than the discrete active types presented here.

Overall, we find that evolved morphologies were able to travel significantly greater distances compared to both random morphologies, and a simple two-cell case. If the distance travelled is averaged over the number of constituent cells in the morphologies, the two-cell morphology in fact achieves the greatest average distance per cell, though at the cost of having highly chaotic trajectories. On the other hand, evolved morphologies display a much lower standard deviation in their travel direction, making their motion much more predictable. This suggests that there may be some trade-off between locomotive efficiency (distance per cell) and reliability in direction of travel. In applications where cells, acting as or carrying a cargo, need to be delivered to a precise area, reliable travel directions would be important; whereas in applications such as area coverage, moving fewer cells greater distances in random directions may suffice, or even benefit.

VI. CONCLUSION

We have shown that artificial evolution can be used to find morphologies that allow simulated groups of connected, contractile cells to locomote consistently in the presence of noise. The patterns shown in the evolved morphologies could inspire future designs for mobile, mirco-scale robots consisting of light-reactive, contractile units. The ability to illicit controlled locomotion from optical illumination will open up new possibilities for achieving swarm-like behaviours in micro-scale systems.

REFERENCES

[1] A. Negro, T. Cherbuin, and M. P. Lutolf, '3D Inkjet Printing of Complex, Cell-Laden Hydrogel Structures,' Scientific Reports, vol. 8, no. 1, Dec. 2018.

[2] S.Kriegman, D. Blackiston, M. Levin, and J. Bongard, 'A scalable pipeline for designing reconfigurable organisms,' Proceedings of the National Academy of Sciences of the USA, Jan. 2020.

[3] S. Wegner, O. I. Sentürk, and J. P. Spatz, 'Photocleavable linker for the patterning of bioactive molecules,' Nature Publishing Group, vol. 5, 2015.

[4] F. G. Downs, D. J. Lunn, M. J. Booth, J. B. Sauer, W. J. Ramsay, R. G. Klemperer, C. J. Hawker, and H. Bayley, 'Multi-responsive hydrogel structures from patterned droplet networks,' Nature Chemistry, 2020.

[5] P. Gobbo, A. J. Patil, M. Li, R. Harniman, W. H. Briscoe, and S. Mann, 'Programmed assembly of synthetic protocells into thermoresponsive prototissues,' Nature Materials, vol. 17, no. 12, Dec. 2018.

[6] A. M. R. Denniss, T. E. Gorochowski, and S. Hauert, 'Augmented reality for the engineering of collective behaviours in microsys- tems,' in Proceedings of MARSS 2019. IEEE Inc., Jul. 2019.

[7] R. Pfeifer and G. Gomez, 'Morphological computation - Connect- ing brain, body, and environment,' in Lecture Notes in Computer Science. Springer, Berlin, Heidelberg, 2009, pp. 66–83.

[8] I. Slavkov, D. Carrillo-Zapata, N. Carranza, X. Diego, F. Jansson, J. Kaandorp, S. Hauert, and J. Sharpe, 'Morphogenesis in robot swarms,' Science Robotics, vol. 3, no. 25, Dec. 2018.

[9] C. Mautner and R. K. Belew, "Evolving robot morphology and control," Artificial Life and Robotics, vol. 4, no. 3, pp. 130–136, Sep. 2000.

[10] V. Vujovic, A. Rosendo, L. Brodbeck, and F. Iida, 'Evolutionary Developmental Robotics: Improving Morphology and Control of Physical Robots,' Artificial Life, vol. 23, no. 2, May 2017.

[11] M. Z. Miskin, A. J. Cortese, K. Dorsey, E. P. Esposito, M. F. Reynolds, Q. Liu, M. Cao, D. A. Muller, P. L. McEuen, and I. Co-hen, 'Electronically integrated, mass-manufactured, microscopicrobots,' Nature, vol. 584, no. 7822, pp. 557–561, Aug. 2020.

[12] C. Lv, S. Namboodiri Varanakkottu, T. Baier, and S. Hardt, 'Controlling the Trajectories of Nano/Micro Particles Using Light-Actuated Marangoni Flow,' America Chemical Society, Nano Lett., 2018.

[13] K. Sims, 'Evolving 3D Morphology and Behavior by Competition,' Artificial Life, vol. 1, no. 4, Jul. 1994.

[14] T. E. Gorochowski, A. Matyjaszkiewicz, T. Todd, N. Oak, K. Kowalska, S. Reid, K. T. Tsaneva-Atanasova, N. J. Savery, C. S. Grierson, and M. di Bernardo, 'BSim: An Agent-Based Tool for Modeling Bacterial Populations in Systems and Synthetic Biology,' PLoS ONE, vol. 7, no. 8, Aug. 2012.

[15] Y. Gu, X. Zhang, Q. Wu, Y. Li, B. Zhang, F. Gao, and Y. Luo, "Research on motion evolution of soft robot based on VoxCAD," in Lecture Notes in Computer Science. Springer Verlag, Aug. 2019.

[16] T. Cickovski, K. Aras, M. S. Alber, J. A. Izaguirre, M. Swat, J. A. Glazier, R. M. Merks, T. Glimm, H. G. E. Hentschel, and S. A. Newman, 'From genes to organisms via the cell a problem-solving environment for multicellular development,' Computing in Science and Engineering, vol. 9, no. 4, pp. 50–60, Jul. 2007.

[17] T. Hirashima, E. G. Rens, and R. M. H. Merks, 'Cellular Potts modeling of complex multicellular behaviors in tissue morphogenesis,' Development, Growth and Differentiation, vol. 59, no. 5, Jun. 2017.